AMERICAN METEOROLOGICAL SOCIETY

Monthly Weather Review

EARLY ONLINE RELEASE

This is a preliminary PDF of the author-produced manuscript that has been peer-reviewed and accepted for publication. Since it is being posted so soon after acceptance, it has not yet been copyedited, formatted, or processed by AMS Publications. This preliminary version of the manuscript may be downloaded, distributed, and cited, but please be aware that there will be visual differences and possibly some content differences between this version and the final published version.

The DOI for this manuscript is doi: 10.1175/2009MWR2683.1

The final published version of this manuscript will replace the preliminary version at the above DOI once it is available.

An observing system experiment for Typhoon Conson (2004) using a singular vector method and DOTSTAR data

Munehiko Yamaguchi *

Japan Meteorological Agency, Tokyo, Japan

Takeshi Iriguchi

Japan Meteorological Agency, Tokyo, Japan

Tetsuo Nakazawa

Meteorological Research Institute, Tsukuba, Japan

Chun-Chieh Wu

National Taiwan University, Taipei, Taiwan

submitted to Monthly Weather Review

(For the Special Collection on "Targeted Observations, Data Assimilation, and Tropical Cyclone Predictability")

* *Corresponding author address:* Munehiko Yamaguchi, 1-3-4 Ote-machi, Chiyoda-ku, Tokyo, 100-8122 Japan

E-mail: munehiko.yamaguchi@gmail.com

ABSTRACT

An Observing System Experiment (OSE) has been performed to investigate the effectiveness of dropwindsonde observations and a sensitivity analysis technique on a typhoon track forecast. Using dropwindsonde observations for Typhoon Conson at 1200 UTC 8 June 2004, which are derived from Dropwindsonde Observation for Typhoon surveillance near the Taiwan Region (DOTSTAR), four numerical experiments are conducted, which are different only in terms of the number of dropwindsonde observations used in a data assimilation system: (I) no observation is assimilated; (II) all observations are assimilated; (III) observations within a sensitive region as revealed by a singular vector method at the Japan Meteorological Agency (JMA) are assimilated; and (IV) observations outside the sensitive region are assimilated. In the comparison of the four track forecasts, Conson's northeastward movement is expressed in the second and third simulations while in the first and fourth experiments Conson stays at the almost same position as its initial position.

Through the OSE, it is found that DOTSTAR observations had a positive impact on the track forecast for Conson, and that observations within the sensitive region are enough to predict the northeastward movement of Conson, indicating that the JMA singular vector method would be useful for the sampling strategy of targeted observations like DOTSTAR.

1. Introduction

During the last few decades there have been significant advances in tropical cyclone (TC) track forecasts along with the remarkable progress of numerical weather prediction (NWP) systems. The verification of TC track forecasts by operational global models has been conducted under the framework of the Working Group on Numerical Experimentation (WGNE) since 1991 (WCRP 1993). For the western North Pacific, for example, it was shown that the annual average position error of four-day forecasts in 2005 (301 km), which are the consensus of the European Centre for Medium-Range Weather Forecasts (ECMWF), the Japan Meteorological Agency (JMA) and the Met Office of the United Kingdom (UKMO), is about the same as that of the two-day forecasts in 1991 (282 km), indicating the success in obtaining a two-day lead time over the past fifteen years (Komori et al. 2007). However, we all know that forecast uncertainty is one key unavoidable aspect of weather forecasting due to the chaotic nature of the atmosphere as well as the imperfection of NWP systems. TC track forecasts are no exception. Consequently, sometimes an almost perfect forecast may only contain position error of less than 50 km in a three-day forecast. However, sometimes the three-day forecast error can be over 1000 km. For this reason, Ensemble Prediction System (EPS) has been attracting much attention because it is expected to provide uncertainty information inherent to each forecast event (e.g. Puri et al. 2001; Yamaguchi et al. 2009).

Meanwhile, there was an attempt to reduce TC track forecast uncertainty itself under THORPEX (The Observing System Research and Predictability Experiment) Pacific Asian Regional Campaign (T-PARC) in 2008. One of the main goals of T-PARC is to lessen forecast uncertainty of TCs which may cause severe weather events on a time scale of one day to two

weeks. For this purpose, dropwindsonde (Hock and Franklin 1999) observations by aircraft were deployed in an effort to understand detailed three dimensional TC structures and TC surrounding environments, and to produce more accurate initial fields for NWP models with the supplementary observation data. In T-PARC, adaptive sampling techniques (Buizza and Montani 1999; Majumdar et al. 2006; Wu et al. 2009) were used, aimed at maximizing the impact of the observations on NWP.

Prior to the above field experiment, we investigated the impact of additional observations on TC track forecasts using JMA's data assimilation and global forecasting system, and the feasibility of adopting a singular vector (SV) method (Palmer et al. 1998) developed at JMA as a sensitivity analysis technique. As for the additional observations, we used Dropwindsonde Observations for Typhoon Surveillance near the Taiwan Region (DOTSTAR) data for Typhoon Conson observed at 1200 UTC 8 June 2004.

Similar surveys have been conducted by Aberson (2003 and 2002), Aberson and Franklin (1999) and Burpee et al. (1996), focusing on hurricanes in the Atlantic and the Eastern and Central Pacific. According to these surveys, it has been found that initial conditions that assimilate all observational data led to statistically better hurricane track forecasts as compared to initial conditions without targeted observations. These studies also demonstrated that adaptive sampling techniques would be useful for the decision-making process on dropwindsonde deployments because TC track forecasts which include observations just within sensitive regions statistically have better performance with respect to those which includes all observations. Following the previous studies, this study aims to evaluate the next two issues:

1. Impact of selected DOTSTAR observations on the track forecast of Conson at 1200 UTC 8 June 2004;

2. Feasibility of the JMA SV method as a sensitivity analysis technique.

For these purposes, two sets of Observing System Experiment (OSE) are performed. In the first OSE (hereafter OSE-1), two initial conditions are created, which are different only in terms of the number of observations used through the data assimilation: one is made without DOTSTAR data; and the other is made with all dropwindsonde data. In the second OSE (hereafter OSE-2), just like OSE-1, two initial conditions are created, which are also different only in terms of observations used during the data assimilation: one is made by assimilating DOTSTAR data within a sensitive region as identified by the JMA SV method; and the other is made using the data outside the sensitive region. We could answer the first question through OSE-1 and the second question through OSE-2.

Section 2 describes DOTSTAR data for Conson and synopsis of the typhoon. Section 3 and 4 describe the experimental designs and the results of OSE-1 and OSE-2, respectively. Section 5 is the discussions of scientific issues on the role of the additional observation data and on what the sensitive region identified by the JMA SV method represents. The conclusions are presented in Section 6.

2. Brief overview of DOTSTAR and Typhoon Conson

a. DOTSTAR project and its data for Typhoon Conson

DOTSTAR is a field experiment conducted by the National Taiwan University and the Central Weather Bureau of Taiwan, along with the National Oceanic and Atmospheric Administration (NOAA) since 2002 (Wu et al. 2005). DOTSTAR has collected adaptive airborne dropwindsonde observations for typhoons which may affect the Taiwan area, aiming at the improvement of typhoon track forecasts with its additional observation data. The observations are available through the Global Telecommunication System (GTS) in real-time, and JMA has used them for its data assimilation since 2004. Studies have shown that the DOTSTAR data have on average improved the 6-72-h track forecasts from operational global models of JMA, NCEP and FNMOC (Fleet Numerical Meteorological and Oceanographic Center) by about 20 % for 10 cases studied in 2004 (Wu et al. 2007a; Chou and Wu 2008).

The Astra SPX jet, which cruises at about 750 km h^{-1} at up to about 14 km with a maximum flight range of about 6.5 hours, is used in this field experiment. Dropwindsondes are released in and around a TC every 150-200 km close to the resolution of the traditional rawinsonde network. In order to maximize the possible improvement of numerical forecasts with the limited aircraft resources, targeted observation techniques are adopted. Three sensitivity analysis products were first taken into consideration to determine the observation strategy: the Deep-Layer Mean (DLM) wind variance using NCEP EPS (Aberson 2003), the Ensemble Transform Kalman Filter based on the 40-member NCEP EPS (ETKF, Majumdar et al. 2002) and SVs by Navy Operational Global Atmospheric Prediction System (NOGAPS, Rosmond 1997; Gelaro et al. 2002; Peng and Reynolds 2006; Reynolds et al.

2008). Along with the progress in DOTSTAR, the fourth method, Adjoint-Derived Sensitivity Steering Vector (ADSSV), has been developed at the National Taiwan University and are currently used for the decision-making of dropwindsonde deployments (Wu et al. 2007b; Wu et al. 2008; Wu et al. 2009).

Sixteen dropwindsondes were released around Conson between 1000 UTC and 1400 UTC on 8 June 2004. The squares and triangles in Figs. 1a - d show the location of dropwindsone observations. As of June 2004, sensitivity analysis guidance mentioned above had not been fully employed yet. Most dropwindsondes were therefore deployed every 150 to 200 km in a circular pattern with its center at Conson's central position, and several dropwindsondes were deployed during the ferry flight. The observation data include wind speed, wind direction, temperature and relative humidity below 195 hPa. As an example, wind observations at 500 hPa and 250 hPa are shown in Figs. 1a and b (a long barb for 5 m s^{-1} and a short barb for 2.5 m s^{-1}), and specific humidity at 500 hPa and 850 hPa are shown in Figs. 1c and d with observation values (g kg^{-1}) indicated beneath each observation point.

b. Synopsis of Typhoon Conson

The best track and intensity of Conson analyzed by the Regional Specialized Meteorological Center (RSMC) Tokyo - Typhoon Center are shown in Fig. 2. Conson formed as a tropical depression in the South China Sea at 1800 UTC 4 June 2004. It moved eastward, then north-northeastward and developed into a tropical storm off the west coast of the Luson island at 1800 UTC 6 June. After that, Conson changed its course toward the northeast and reached typhoon intensity at 0600 UTC 8 June. Remaining moving at the same direc-

tion, Conson reached the peak intensity with the maximum sustained wind of 80 knots at 1200 UTC 9 June. It made landfall over Shikoku at 0700 UTC 11 June with tropical storm strength (RSMC Tokyo - Typhoon Center 2004). As one of the eleven typhoons landing on Japan in 2004, Conson caused a torrential rainfall of 40 mm hour^{-1} in Kochi and 85 mm hour^{-1} in Tanegashima.

To understand the synoptic environment at 1200 UTC 8 June 2004, the analysis field of wind and geopotential height at 500 hPa and 250 hPa are shown in Figs. 3a and b. These are the results of JMA four dimensional variational assimilation system (4D-VAR, Kadowaki 2005; JMA 2007) (the analysis fields shown in Figs. 3a and b were produced without DOTSTAR data). Figure 3a shows that Conson was located at the west edge of the Pacific High, and Fig. 3b shows that it was located at just south of the westerly jet with its axis lying on the west side against Conson's central position: the westerly wind with a little southerly flow was present just north of Conson. As these figures show, Conson was in a confluent area induced by the westerly jet and the southerly flow at the west edge of the Pacific High. These are the remarkable characteristics of the synoptic environment around Conson at 1200 UTC 8 June when DOTSTAR observation was conducted.

3. OSE-1: Impact of dropwindsonde observations on Conson's track prediction

a. Experimental description

OSE-1 is performed to investigate the impact of additional observations on Conson's track prediction. For this purpose, JMA's operational NWP system for global forecasting as of February 2005 is used: the 4D-VAR system for data assimilations (the resolutions of the inner and outer model are T63L40 and TL319L40, respectively) and the Global Spectral Model (TL319L40) for numerical integrations. Two initial conditions are produced, which are different only in terms of the number of observations used in the data assimilation: one is made without DOTSTAR data and the other is made using all of the data (hereafter, the experiment in which no DOTSTAR data is assimilated is referred to as NODROP, and the other with all DOTSTAR data assimilated is referred to as ALLDROP).

b. Results of OSE-1

The results of OSE-1 are shown in Fig. 4 and Table 1. The thin (thick) solid line is a track forecast of NODROP (ALLDROP). Comparison of these two tracks indicates that ALLDROP can capture Conson's northeastward movement despite of a strong slow bias. On the other hand, Conson heads toward north and finally disappears just after making landfall on Taiwan in NODROP. Verification against the best track by RSMC Tokyo - Typhoon Center shows that the position errors of NODROP and ALLDROP are 410 km and 181 km for 24-h forecast, respectively. This result demonstrates that DOTSTAR data show a very

positive impact on improving Conson's track prediction at 1200 UTC 8 June 2004.

c. Differences of the initial conditions between NODROP and ALLDROP

In this section we focus on the differences of the initial conditions used in NODROP and ALLDROP in order to understand how the inclusion of the dropwindsonde data leads to the different track prediction. As mentioned in Section 3a, the initial conditions are the only thing that is different between NODROP and ALLDROP. Therefore, the differences between them would help us understand why ALLDROP results in a better track prediction.

Figure 5 shows the analysis increments resulting from assimilating all dropwindsonde data in ALLDROP. The increments are represented as a form of the vertical distribution of each component of the total energy (the increments at each vertical level are the result of summing up increment over the global domain though the increments appear only around the typhoon because the assimilation of dropwindsonde data is the only difference between NODROP and ALLDROP). Here, the total energy norm including a specific humidity term (Barkmeijer et al. 2001) is used:

$$
\begin{aligned}
(\mathbf{x}, \mathbf{E}\mathbf{x}) \;=\; & \frac{1}{2}\int_0^1 \int_S (\nabla\Delta^{-1}\zeta_x \cdot \nabla\Delta^{-1}\zeta_x + \nabla\Delta^{-1}D_x \cdot \nabla\Delta^{-1}D_x \\
& + \frac{c_p}{T_r}T_x T_x \\
& + w_q \frac{L_c^2}{c_p T_r} q_x q_x) dS \left(\frac{\partial p}{\partial \eta}\right) d\eta \\
& + \frac{1}{2}\int_S \frac{R_d T_r}{P_r} P_x P_x dS
\end{aligned}
\tag{1}
$$

with ζ_x, D_x, T_x, q_x and P_x being the vorticity, divergence, temperature, specific humidity

and surface pressure components of a perturbation $\mathbf{x}$. c_p is the specific heat of dry air at constant pressure, L_c is the latent heat of condensation and R_d is the gas constant for dry air. T_r = 300K is a reference temperature, P_r = 800 hPa is a reference pressure and w_q is a constant (w_q = 1 in this study). As shown in Fig. 5, the analysis increments are mainly explained by the vorticity component of energy from middle to upper troposphere with its peak at vertical level 22 and the specific humidity component from lower to middle troposphere (In Fig. 5, vertical level 7, 15 and 22 nearly correspond to 850, 500 and 250 hPa, respectively). Compared with the above two variables, the increments in temperature and divergence are relatively small.

Figures 6a - e show the horizontal distributions of the analysis increments in ALLDROP. The vertically accumulated total energy of the analysis increments is given in Fig. 6a, its vorticity and specific humidity components are given in Figs. 6b and c, and wind vectors and isotachs at 250 hPa and 500 hPa are given in Figs. 6d and e, respectively. As shown in Figs. 6b, d and e, the vorticity increments consist of three vortical structures: (1) a cyclonic circulation at the northeast region against Conson's central position; (2) an anticyclonic circulation at the opposite side; and (3) another anticyclonic circulation about 500 km east of Conson's central position. It should be noted that the peak points of the vorticity increments are not necessarily consistent with the area where the wind increments have large amplitudes.

Figures 7a - d show the initial fields of NODROP and ALLDROP regarding vorticity (shaded) and streamline (arrow) at 250 hPa (left) and 500 hPa (right). There are two major differences at the 250-hPa level; one is that the location of maximum vorticity in ALLDROP is shifted to the best track position of Conson, likely owing to the use of all dropwindsonde

information surrounding Conson, and the other is the steering flow associated with the west edge of the Pacific High. The steering flow in NODROP is from south to north, which is almost same as the direction of the forecast track as shown in Fig. 4. For ALLDROP, on the other hand, the flow is from southwest to northeast, which is consistent with the direction of the motion of Conson simulated in ALLDROP. This flow change is the most prominent at 250 hPa, but it can be also seen from about 200 hPa to 500 hPa though the impact becomes less distinct away from the 250-hPa level.

Figures 8a - f show the initial fields of NODROP and ALLDROP and the differences between them, regarding specific humidity at 500 hPa (left) and 850 hPa (right), where analysis increments are relatively large. Compared with observations shown in Figs. 1c and d, it is revealed that the initial field of NODROP has less moisture content almost all around the typhoon at both middle and lower model levels. By assimilating the dropwindsonde observations, however, these inadequate expressions are improved and the initial expression of the moisture field in ALLDROP becomes close to the observations from the DOTSTAR soundings.

4. OSE-2: Feasibility of adopting JMA's singular vector method as a sensitivity analysis technique

a. Experimental description

Another OSE, OSE-2, is performed to investigate the feasibility of adopting JMA's SV method as a sensitivity analysis technique. Just like OSE-1, two initial conditions are pro-

duced, which are different only in terms of observations used in the data assimilation: one is made with DOTSTAR data within a sensitive region as revealed by the SV method (hereafter, referred to as SVDROP) and the other is made using the data outside the sensitive region (hereafter, referred to as NSVDROP). The other configurations such as the 4D-VAR data assimilation system and the NWP model (Global Spectral Model with TL319L40) are exactly the same as those used in OSE-1.

b. Singular Vector Method at JMA

Under the assumption that a perturbation grows linearly, a SV with a large singular value represents a fast-growing perturbation (Lorenz 1965). Consider a growth rate of a perturbation $\mathbf{x}$ as shown in (2):

$$\frac{\| \mathbf{x}(t = t_a) \|}{\| \mathbf{x}(t = t_0) \|} \qquad \mathbf{x} \in R^n, \tag{2}$$

where $\mathbf{x}(t = t_0)$ is a perturbation at a base time t_0, $\mathbf{x}(t = t_a)$ is one at an optimization time $t_a (t_a > t_0)$ and $\| \cdot \|$ denotes the norm associated with the Euclidean inner product. The growth rate of a perturbation given by Eq. (2) changes into Eq. (3), using a tangent forward propagator $\mathbf{M}$:

$$\frac{\| \mathbf{x}(t = t_a) \|}{\| \mathbf{x}(t = t_0) \|} = \sqrt{\frac{(\mathbf{TMx}(t = t_0), \mathbf{E_f TMx}(t = t_0))}{(\mathbf{x}(t = t_0), \mathbf{E_i x}(t = t_0))}}, \tag{3}$$

where $\mathbf{E_i}$ and $\mathbf{E_f}$ are norm operators at t_0 and t_a, respectively. The local projection operator $\mathbf{T}$ makes a vector to zero outside a prescribed domain, which enables to calculate perturbations with maximum amplitude at t_a over the targeted area. $(,)$ denotes the Eulerian inner

product. The growth rate equation still changes to Eq. (4) and (5) from Eq. (3), using $\hat{\mathbf{x}} = \mathbf{E_i}^{\frac{1}{2}}\mathbf{x}(t = t_0)$, $\mathbf{A} = \mathbf{E_f}^{\frac{1}{2}}\mathbf{TME_i}^{-\frac{1}{2}}$ and adjoint matrix represented by the superscript $*$:

$$\frac{\parallel \mathbf{x}(t = t_a) \parallel}{\parallel \mathbf{x}(t = t_0) \parallel} = \sqrt{\frac{(\hat{\mathbf{x}}, (\mathbf{E_f}^{\frac{1}{2}}\mathbf{TME_i}^{-\frac{1}{2}})^{*}\mathbf{E_f}^{\frac{1}{2}}\mathbf{TME_i}^{-\frac{1}{2}}\hat{\mathbf{x}})}{(\hat{\mathbf{x}}, \hat{\mathbf{x}})}}, \tag{4}$$

$$= \sqrt{\frac{(\hat{\mathbf{x}}, \mathbf{A}^{*}\mathbf{A}\hat{\mathbf{x}})}{(\hat{\mathbf{x}}, \hat{\mathbf{x}})}}. \tag{5}$$

Eq. (5) represents that SVs, or forward SVs of matrix $\mathbf{A}$, grow up about a given trajectory with their growth rates of the corresponding singular values. Therefore the first SV, which has the largest singular value, maximizes the ratio in Eq. (2) and the second SV gives the fastest-growing perturbation following the first SV, and so on. These SVs are the solutions of the eigenvalue problem shown in Eq. (6):

$$\mathbf{A}^{*}\mathbf{A}\hat{\mathbf{x}} = \lambda\hat{\mathbf{x}} \qquad (\lambda : \text{eigenvalue}). \tag{6}$$

In this study, $\mathbf{M}$ and $\mathbf{M}^{*}$ are the tangent-linear and adjoint models used for the 4D-VAR data assimilation system at JMA, which has been in operation since February 2005 (Kadowaki 2005). The resolutions are T63L40. They consist of dynamics based on Eulerian integrations and physical processes containing representations of vertical diffusion, gravity wave drag, large-scale condensation, long-wave radiation and deep cumulus convection. Two kinds of SVs can be calculated: one is dry SVs and the other is moist SVs. The dry SVs, which are expected to identify the dynamically most unstable mode of the atmosphere like the baroclinic mode, are obtained using the simplified physical process which only includes vertical diffusion. For the moist SVs that are computed using the full physical process, they

can capture the uncertainty in the area such as a tropical region or a TC surrounding where moist processes are crucial (Barkmeijer et al. 2001; Puri et al. 2001; Kim and Jung 2008). Both SVs are computed applying an iterative Lanczos procedure (e.g. Strang 1986) to the linear propagator **M** instead of solving Eq. (6) directly.

c. Singular Vector Calculation for Typhoon Conson

A moist SV calculation is performed targeting Conson. The initial time is 1200 UTC 8 June 2004, when DOTSTAR conducted its airborne observation. The optimization time interval $t_a - t_0$ is 24 hours: the optimization time is 1200 UTC 9 June 2004. The targeted region is a rectangle, 10 degrees in longitude and 5 degrees in latitude with its center at Conson's analyzed position at the evaluation time, 23.3N, 123.8E. The initial condition for the SV calculation is produced by interpolating an analysis field with TL319L40 resolution which does not include any DOTSTAR data.

Following the results of OSE-1, we eliminate the effects of temperature and divergence from the total energy at the initial time when carrying out the SV calculation. In addition, the influence of specific humidity is limited below model level 20 (about 300 hPa level). In the final norm, only the effect of vorticity under model level 15 (about 500 hPa level) is evaluated to focus on the representation of a TC. Figures 9a and b show the vertically accumulated energy of the first moist SV at the initial and evaluation time, respectively. Amplitudes in both figures are normalized by the maximum value in the field. It is found that the large amplitudes extend from north to southeast about 200 km to 500 km away from Conson's central position in the initial SV, and that there exists a TC-like cyclonic

structure whose center is close to the analyzed position of Conson at the evaluation time in the final SV. The sensitive region is related to synoptic features such as the western edge of the Pacific High, the westerly jet just north of Conson and a convective area in the outer bands southeast of the typhoon (see Section 5a for more details).

When the initial condition of SVDROP is produced, eight observation points, half the number of the total observation points, are selected in the order corresponding to the amount of the total energy, or sensitivity. As a result, the squares in Fig. 1 are selected for SVDROP while the other half of the data (triangles in Fig. 1) are selected when producing the initial condition of NSVDROP.

d. Results of OSE-2

The results of OSE-2 are shown in Fig. 4 and Table 1. The thick (thin) dot line is the track forecast of SVDROP (NSVDROP). In the comparison of these two tracks, SVDROP shows Conson's northeastward movement similar to ALLDROP. On the other hand, the typhoon dissipates near Taiwan in NSVDROP just like NODROP. This result demonstrates that in this particular case, DOTSTAR data within the sensitive region is all it takes to capture Conson's movement toward the northeast, and that the sensitivity analysis guidance using the JMA SV method appears effective for targeted observations of typhoons such as in DOTSTAR.

e. Characteristics of the initial conditions of SVDROP and NSVDROP

Figures 7e - h show the initial fields of SVDROP and NSVDROP, regarding the vorticity (shaded) and streamline (arrow) fields at 250 hPa (left) and 500 hPa (right). Not assimilating observations in a circular pattern fully around Conson, the initial field of SVDROP at 250 hPa does not produce the vorticity shift as shown in ALLDROP. However, SVDROP has the same characteristic as ALLDROP in resolving the critical southwesterly wind as seen in the southeastern side of Conson. Just like in ALLDROP, the flow change is the most prominent at 250 hPa, and the influence becomes weaker in proportion to the distance from the 250-hPa level. On the contrary, the southerly wind is dominant at the corresponding region in NSVDROP which fails to realize Conson's northeastward movement. We believe this is the essential difference in the model's initial condition leading to the completely dissimilar two groups of track forecasts in ALLDROP/SVDROP and NODROP/NSVDROP.

Figures 8g -j show the differences of the initial fields between SVDROP and NODROP, and the differences between NSVDROP and NODROP, regarding specific humidity at 500 hPa (left) and 850 hPa (right). In response to the observations assimilated, there exists the enhancement of specific humidity from the southeast to north area of Conson from the lower to middle levels in the initial field of SVDROP, which is almost the same characteristic as ALLDROP as seen in Figs. 8e and f. On the other hand, the increased specific humidity is limited from northwest to south in NSVDROP.

Through OSE-1 and OSE-2, it is found that the common features of the initial conditions in both ALLDROP and SVDROP, where Conson's track forecasts are improved, are the northeastward steering flow from the middle to the upper troposphere, which is associated

with the west edge of the Pacific High, and the enhancement of specific humidity from the southeast to north of Conson from the lower to middle troposphere. Although it would be difficult to identify exactly what element and which area may have contributed to the improvement of the track forecast, our understanding on the steering flow (Wu et al. 2003; 2004) suggests that the analysis increments causing the modification of the wind field should have played an important role in Conson's northeastward movement prediction. In addition, the area of specific humidity increments includes the convective area in the outer bands of the typhoon, indicating that the improvement of outer structure representation might also play a role in the track change. In fact, as will be shown in Section 5a, the specific humidity component of the first SV is also found to be important.

5. Discussions

a. SV structure

To more closely examine the effectiveness of the JMA SV method as a sensitivity analysis technique, this section focuses on what the SV shown in Fig. 9a reflects and how well it explains the analysis increments in ALLDROP and SVDROP, where Conson's track forecasts are improved.

Before going into the details about the structure of the SV, the validity of the linear growth assumption of the SV calculation is investigated by the study of the similarity index proposed by Buizza (1994). The similarity index is a value of inner product of two vectors, and therefore, by considering an evolved SV and a nonlinearly growing SV as the two vectors,

the similarity of those two vectors can be examined. Here, the evolved SV is the result of integrating the first SV up to the evaluation time with the T63L40 tangent-linear model, and the nonlinearly growing SV is the result of operating a norm operator at the evaluation time, $\mathbf{E_f}$, to the differences between the non-perturbed run and the perturbed run at the evaluation time, where both runs are based on the T63L40 non-linear model, and the first SV is used as an initial perturbation in the perturbed run. The amplitudes of the initial perturbation are determined in the same way as the Typhoon Ensemble Prediction System (TEPS) at JMA (Yamaguchi et al. 2009) so that the maximum value of the zonal or meridional wind perturbations is equal to 6 m s^{-1} (approximately same amplitude as analysis increments shown in Fig. 6e). The similarity index of the above setting is 0.95. This high similarity index denotes that the linear growth assumption is well maintained during the evaluation time interval, and that the initial SV is expected to grow in a non-linear model as is the case with a linear model up to the evaluation time.

Figure 10 shows the vertical energy distribution of the initial SV. The initial SV is mainly explained by the vorticity component with the highest energy at model level 14 (about 540 hPa level). Figure 11a shows the vertically accumulated vorticity component of energy of the initial SV, and Figs. 11b and c show the wind vectors and isotachs at 250 hPa and 500 hPa, where the SV is amplified in the same way as TEPS. As shown in Figs. 11a, b and c, the vorticity perturbation consists of two vortical structures: (1) a large cyclonic circulation extending from the northwest to east relative to Conson's central position; and (2) an anticyclonic circulation to the south of Conson. Regarding the wind field, the south to east side of Conson has an eastward component just like in ALLDROP (Figs. 6d and e). When the analysis increments of vorticity in ALLDROP (Fig. 6b) are compared to

the SV vorticity structure, it is shown that both have high similarity. In actuality, the SV being used as an initial perturbation and added to the initial field of NODROP (the amplitudes are determined in the same way as TEPS), the southerly winds at the eastern side of Conson have changed to the southwesterly wind, which is the very characteristic in ALLDROP and SVDROP (Figs. 7i and j). This result confirms that the SV succeeds in capturing a sensitive region which may have a large impact on forecasting as seen in the differences between ALLDROP/SVDROP and NODROP/NSVDROP.

Figure 12a shows the vertically accumulated specific humidity component of energy of the initial SV. The area with large amplitudes is seen in the southeast region about 300km away from the central position, where outer bands exist. Figures 12b and c show the vertically accumulated specific humidity component of energy of the initial and final SVs which are calculated under the condition that only the effect of specific humidity is considered in a formulation of an initial norm (in the final norm, as in the SV calculation mentioned at Section 3c, only the effect of vorticity under model level 15 is considered just to focus on the representation of a TC). By studying the final SV, we can see a TC-like cyclonic structure whose center is close to the analyzed position of Conson at the evaluation time. In addition, Figs. 12a and b have a quite similar structure. Therefore, it can be inferred that specific humidity perturbation at around the southeastern side of Conson would also play an important role in the track forecast. In T-PARC, dropwindsonde observations were collected not only in the usual environment of the TC as has been routinely sampled by DOTSTAR but also outer regions approximately 300 km or more away from the TC center. These observations would help us understand through another set of OSEs how sampling convective regions related to the outer bands of TCs affects track forecasting.

Finally, to evaluate whether the SV in Fig. 9a really explains the error growth of Conson, we conduct another numerical experiment starting from an initial condition perturbed by the SV (hereafter, referred to as SVPTB). Following the same method as TEPS, the SV is added to the initial field in NODROP with the maximum value of the zonal or meridional wind perturbations set to 6 m s^{-1} and then specific humidity perturbation 0.8 g kg^{-1}. The result of SVPTB is shown in Fig. 4 and Table 1. SVPTB succeeds in realizing Conson's northeastward movement as in both ALLDROP and SVDROP. This result supports that the SV well explains the analysis increments in ALLDROP and SVDROP.

Compared with the track forecasts in both ALLDROP and SVDROP, SVPTB considerably improves the slow and northeastward track bias. This may result from the perturbation around the westerly jet. As shown in Figs. 3a and b, Conson was located in a confluent area induced by the westerly jet and the southerly flow at the west edge of the Pacific High at 1200 UTC 8 June when DOTSTAR observations were conducted. Figure 13 shows the 500 hPa geopotential height of SVPTB (thick) and NODROP (thin) at the initial time. Compared with NODROP, the axis of the westerly jet in SVPTB moves to south, which may have caused more close interaction between the jet and Conson and thus have favored the northeastward movement of the typhoon. Therefore, it is proposed, if additional observations had been performed around such areas with the westerly jet as shown in the SV in Fig. 9a, the track forecast in ALLDROP and SVDROP would have had been further improved.

In all, considering that the moist SV calculated for this study has the similar structure as the analysis increments in ALLDROP and SVDROP, where Conson's track forecasts are improved, and that it has a positive impact on Conson's track forecast when it is used as an initial perturbation, we could conclude that the SV was successful in identifying a sensitive

region which could potentially lead to large TC track forecast error reduction and that the JMA SV method would be useful for the sampling strategy for targeted observations in the field programs such as DOTSTAR and T-PARC.

b. Implications for targeted observations

The sensitivity analysis calculation in this study is different from that in real targeted observations as in T-PARC and DOTSTAR. We have adopted the most favorable conditions in order for the leading JMA SV to identify a sensitive region. Firstly, the initial condition for the SV computation comes from an analysis field, not a forecast field that is necessary given the time required to notify officials about deployments. Secondly, there are constraints on the norm definition. Finally, the analysis TC position at the evaluation time is used to set a targeted area. The reason why we have used these conditions is to confirm if JMA SVs are successful in capturing a sensitive region under the easiest conditions. In that sense, this study is at a starting point to verify the feasibility of JMA SVs as sensitivity analysis guidance. Using recently collected data from T-PARC, we will further verify the effectiveness of the guidance actually used in T-PARC.

In the case of Conson, unfortunately, it seems to be quite difficult to identify the sensitive region if we used forecast data, not analysis data, as an initial condition for the SV computation because the expression of the typhoon in the forecast field is very weak. As for the actual impact of the norm constraints, removing the effect of temperature and divergence component from the initial and final norm has little influence, but the limitation of vertical integration in the final norm changes the result. Without the limitation, the first SV is

related to the development of the jet itself, not the TC. A TC-related SV as seen in Fig. 9 is calculated as the second SV. The change of a targeted area into a box with its center at a forecast position by NODROP at the evaluation time also changes the original first SV to the fourth SV, the first to third SVs being related to the jet. These results imply that it is important to define a sensitive region for the TC after evaluating whether or not the final SVs are associated with the TC.

While the vorticity component of the analysis increments has the maximum value around 250 hPa (Fig. 5), that of the first SV has a peak around 500 hPa (Fig. 10). This difference would come from the fact that the SV does not explain the vorticity shift at 250 hPa, and that the analysis increments do not appear near the jet. However, both are successful in representing the southwesterly steering flow which we believe should have played a critical role in improving the track forecast. As Bergot et al. (1999) and Aberson (2003) indicate, that may imply that targeted observations should be performed with a broad vertical and horizontal coverage, not only focusing on the point with the maximum sensitivity, because such flows also have a three dimensional structure.

6. Conclusions

Dropwindsondes were deployed under the DOTSTAR project in an attempt to improve a track forecast of Typhoon Conson at 1200 UTC 8 June 2004. We have studied the impact of the dropwindsonde observations on the typhoon track forecast and the feasibility of adopting JMA's singular vector method as a sensitivity analysis technique. Using an operational NWP system for global forecasting at JMA, four numerical experiments, which are different in

terms of the number of observations used in the 4D-VAR assimilation system, are conducted. The results reveal that the observation data have a significantly positive impact on the track forecast, and that the calculated SV appears successful in representing the sensitive region that leads to large forecast error reduction.

The common features of the initial conditions which succeed in realizing Conson's northeastward movement are (1) the southwesterly steering flow from middle to upper troposphere which are associated with the west edge of the Pacific High; and (2) the enhancement of specific humidity from the southeast to the north area of Conson from lower to middle troposphere.

Looking into the structures of the calculated SV, it turns out that the SV has the similar characteristics to the above features. In reality, when the SV is used as an initial perturbation, the perturbed run succeeds in realizing Conson's northeastward movement. The track forecast of the perturbed run had the best performance, which may indicate that the SV that was also perturbing the westerly jet favors the typhoon to move northeast. Therefore, we would presume that if additional observations had been performed around such areas as the westerly jet, the track forecast adding the data should have had much more improvement.

Our future plan is to evaluate more cases in order to obtain statistical significance and to understand the influence of targeted observations on TC forecasts. This can be achieved through the T-PARC field program in the summer of 2008 and future field campaigns.

Acknowledgments.

DOTSTAR is supported through the National Science Council of Taiwan by Grants

NSC94-2119-M-002-006-AP1, NSC94-2745-P-002-002, NSC95-2119-M-002-039-MY2, the Office of Naval Research Grant N00014-05-1-0672, and MOTC-CWB-96-6M-02. Special thanks are given to Sharan Majumdar of University of Miami for his helpful comments.

REFERENCES

Aberson, S. D., 2002: Two years of operational hurricane synoptic surveillance. *Wea. Forecasting.*, **17**, 1101-1110.

Aberson, S. D., 2003: Targeted observations to improve operational tropical cyclone forecast guidance. *Mon. Wea. Rev.*, **131**, 1613-1628.

Aberson, S. D., and J. L. Franklin, 1999: Impact of hurricane track and intensity forecasts of GPS dropwindsonde observations from the first-season flights of the NOAA Gulfstream-IV jet aircraft. *Bull. Amer. Meteor. Soc.*, **80**, 421-427.

Barkmeijer, J., Buizza, R., Palmer, T. N., Puri, K. and Mahfouf, J. F., 2001: Tropical singular vectors computed with linearized diabatic physics. *Quart. J. Roy. Meteor. Soc.*, **127**, 685-708.

Bergot T., G. Hello, A. Joly, and S. Malardel, 1999: Adaptive observations: A feasibility study. *Mon. Wea. Rev.*, **127**, 743-765.

Buizza, R., 1994: Sensitivity of optimal unstable structures. *Quart. J. Roy. Meteor. Soc.*, **120**, 429-451.

Buizza, R., and A. Montani, 1999: Targeting observations using singular vectors. *J. Atmos Sci.*, **56**, 2965-2985.

Burpee, R. W., J. L. Franklin, S. J. Lord, R. E. Tuleya, and S. D. Aberson, 1996: The impact of Omega dropwindsondes on operational hurricane track forecast models. *Bull. Amer. Meteor. Soc.*, **77**, 925-933.

Chou K.-H., and C.-C. Wu, 2008: Development of the typhoon initialization in a mesoscale model - Combination of the bogused vortex with the dropwindsonde data in DOTSTAR. *Mon. Wea. Rev.*, **136**, 865-879.

Gelaro, R., T. E. Rosmond, and R. Daley, 2002: Singular vector calculations with an analysis error variance metric. *Mon. Wea. Rev.*, **130**, 1166-1186.

Hock, T. F. and J. L. Franklin, 1999: The NCAR GPS Dropwindsonde, *Bull. Amer. Meteor. Soc.*, **80**, 407-420.

JMA, 2007: Outline of the operational numerical weather prediction at the Japan Meteorological Agency. Appendix to WMO Numerical Weather Prediction Progress Report. Japan Meteorological Agency, Tokyo, Japan. Available online at `http://www.jma.go.jp/jma/jma-eng/jma-center/nwp/outline-nwp/index.htm`

Kadowaki, T., 2005: A 4-dimensional variational assimilation system for the JMA Global Spectrum Model *CAS/JSC WGNE Research Activities in Atmospheric and Oceanic Modelling*, **34**, 1-17.

Kim. H. M., and B.-J. Jung, 2008: Influence of physical processes and norm on singular vectors of tropical cyclone. *Mon. Wea. Rev.* (accepted)

Komori, T., M. Yamaguchi, R. Sakai, and Y. Takeuchi, 2007: WGNE Intercomparison of Tropical Cyclone Forecasts with Operational Global Models: Quindecennial Report. *Science Highlights*, WCRP. Available online at `http://wcrp.wmo.int/documents/WGNE_TC_Intercomparison_Quindecennial_Quicklook15Anniversary.pdf`.

Lorenz, E. N., 1965: A study of the predictability of a 28-variable atmospheric model. *Tellus*, **17**, 321-333.

Majumdar, S. J., C. H. Bishop, B. J. Etherton, and Z. Toth, 2002: Adaptive sampling with the ensemble transform Kalman filter. Part II: Field program implementation. *Mon. Wea. Rev.*, **130**, 1356-1369.

Majumdar, S. J., S. D. Aberson, C. H. Bishop, R. Buizza, M. S. Peng and C. A. Reynolds, 2006: A comparison of adaptive observing guidance for Atlantic tropical cyclones. *Mon. Wea. Rev.*, **134**, 2354-2372.

Palmer, T. N., R. Gelaro, J. Barkmeijer, and R. Buizza, 1998: Singular vectors metrics, and adaptive observations. *J. Atmos. Sci.*, **55**, 633-653.

Peng, M. S., and C. A. Reynolds, 2006: Sensitivity of Tropical Cyclone Forecasts as Revealed by Singular Vectors. *J. Atmos. Sci.*, **63**, 2508-2528.

Puri, K., J. Barkmeijer, and T. N. Palmer, 2001: Ensemble prediction of tropical cyclones using targeted diabatic singular vectors. *Quart. J. Roy. Meteor. Soc.*, **127**, 709-731.

Reynolds, C. A., M. S. Peng, and J.-H. Chen, 2008: Recurving tropical cyclones: singular vector sensitivity and downstream impacts. *Mon. Wea. Rev.* (accepted)

Rosmond, T. E., 1997: A technical description of the NRL adjoint model system, NRL/MR/7532/7230, 62pp.

RSMC Tokyo-Typhoon Center, 2004: Annual Report on Activities of the RSMC Tokyo-Typhoon Center, 61pp.

Strang, G., 1986: Introduction of Applied Mathematics. Wellesley-Cambridge Press, 758pp.

WCRP, 1993: Report of the eight session of the CAS/JSC Working Group on Numerical Experimentation, Washington D. C., USA, 2-6 November 1992, WMO/TD No. 549, 41pp,

WMO.

Wu, C.-C., T.-S. Huang, W.-P. Huang, and K.-H. Chou, 2003: A new look at the binary interaction: Potential vorticity diagnosis of the unusual southward movement of Typhoon Bopha (2000) and its interaction with Typhoon Saomai (2000). *Mon. Wea. Rev.*, **131**, 1289-1300.

Wu, C.-C., T.-S. Huang, and K.-H. Chou, 2004: Potential vorticity diagnosis of the key factors affecting the motion of Typhoon Sinlaku (2002), *Mon. Wea. Rev.*, **132**, 2084-2093.

Wu, C.-C., P.-H. Lin, S. D. Aberson, T.-C. Yeh, W.-P. Huang, J.-S. Hong, G.-C. Lu, K.-C. Hsu, I-I Lin, K.-H. Chou, P.-L. Lin, and C.-H. Liu, 2005: Dropwindsonde Observations for Typhoon Surveillance near the Taiwan Region (DOTSTAR): An Overview. *Bull. Amer. Meteor. Soc.* **86**, 787-790.

Wu, C.-C., K.-H. Chou, P.-H. Lin, S. D. Aberson, M. S. Peng, and T. Nakazawa, 2007a: The impact of dropwindsonde data on typhoon track forecasts in DOTSTAR, *Weather and Forecasting*, **22**, 1157-1176.

Wu, C.-C., J.H. Chen, P.H. Lin, and K.H. Chou, 2007b: Targeted Observations of Tropical Cyclone Movement Based on the Adjoint-Derived Sensitivity Steering Vector. *J. Atmos. Sci*, **64**, 2611-2626.

Wu C.-C., S.-G. Chen, J.-H. Chen, and K.-H. Chou, 2008: Typhoon-Trough Interaction from both Adjoint-Derived Sensitivity Steering Vector (ADSSV) and Potential Vorticity (PV) Perspectives. *Mon. Wea. Rev.* (in press)

Wu, C.-C. and Coauthors, 2009: Intercomparison of targeted observation guidances for tropical cyclones in the western North Pacific. *Mon. Wea. Rev.* (accepted)

Yamaguchi, M., R. Sakai, M. Kyoda, T. Komori, and T. Kadowaki, 2009: Typhoon Ensemble Prediction System developed at the Japan Meteorological Agency. *Mon. Wea. Rev.* (accepted)

List of Figures

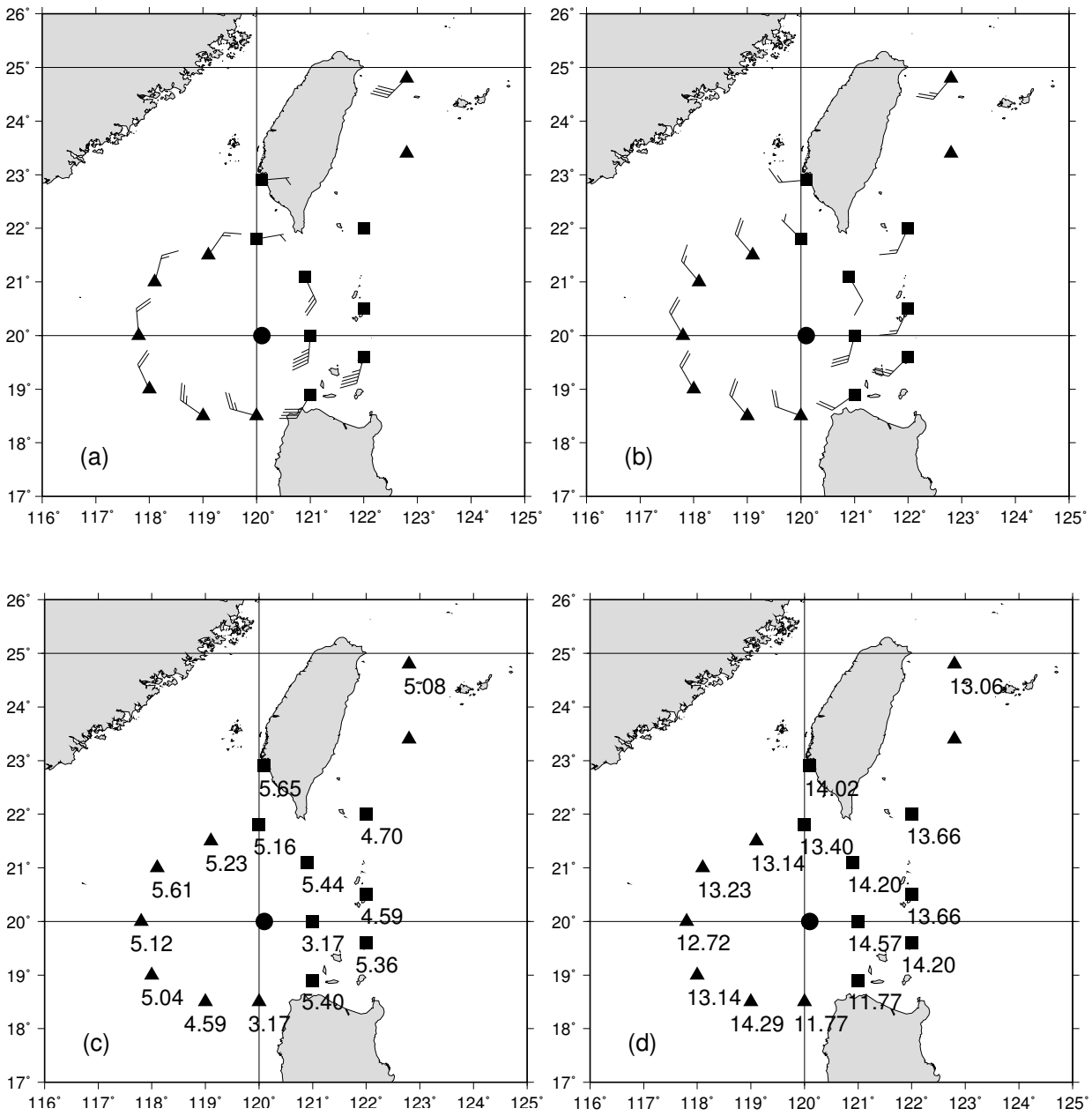

FIG. 1. DOTSTAR observations at 1200 UTC 8 June 2004 (square and triangle points): (a) 500 hPa wind, (b) 250 hPa wind, (c) 500 hPa specific humidity and (d) 850 hPa specific humidity. In (a) and (b), a long barb represents 5 m s^{-1} and a short barb does 2.5 m s^{-1}. In (c) and (d), the observation values (g kg^{-1}) are indicated under each observation point. No line or value is shown at points of missing data. The black dot represents the analyzed central position of Conson.

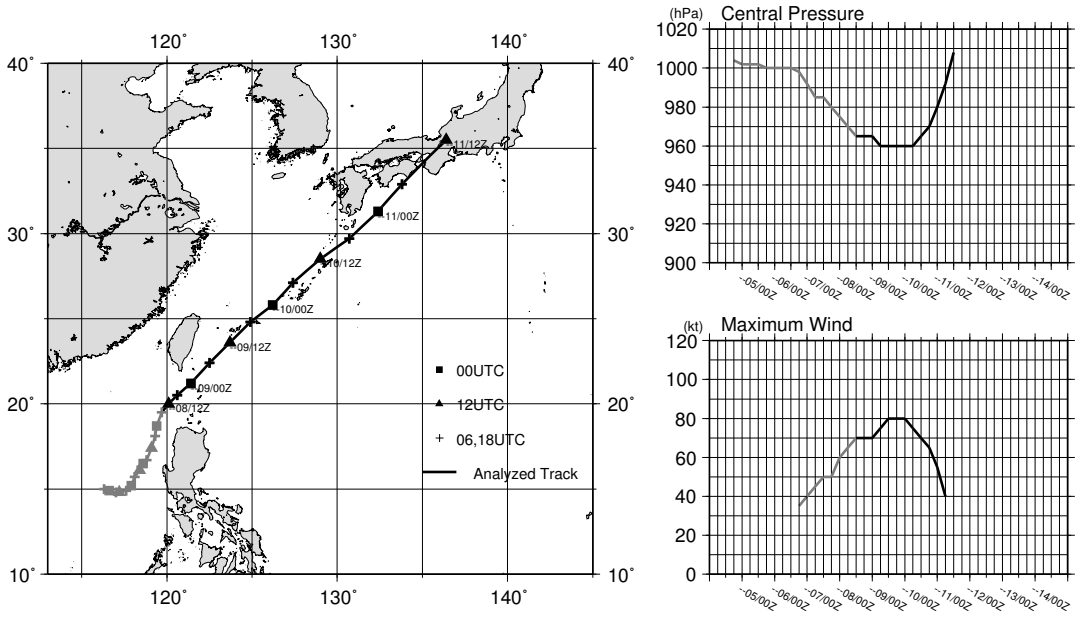

FIG. 2. Analyzed track and intensity of Conson. The figure on the left shows the analyzed track of Conson from 1800 UTC 4 June 2004 (time of genesis) to 1200 UTC 11 June 2004. From the genesis time to the observation time, 1200 UTC 8 June 2004, the line is shown in grey color and after that it is shown in black color. Figure on the upper and lower right show the analyzed intensity: central pressure (hPa) and maximum wind (kt), respectively.

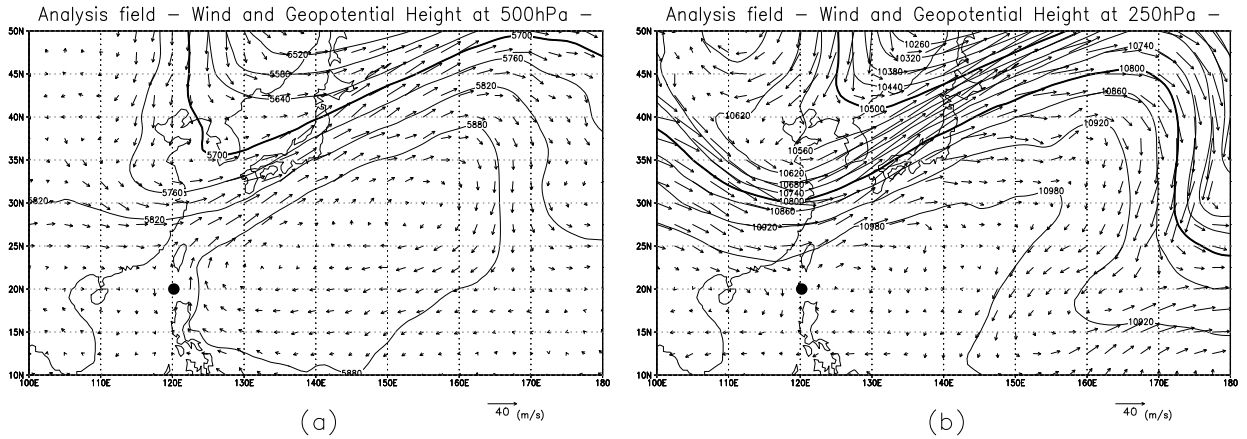

FIG. 3. Synoptic environment around Conson at 1200 UTC 8 June 2004. Wind (m s^{-1}) and geopotential height (m) at (a) 500 hPa and (b) 250 hPa are shown. Wind is given with vector (the scale is shown at lower right on each figure) and geopotential height is given with line. The black dot represents the analyzed central position of Conson.

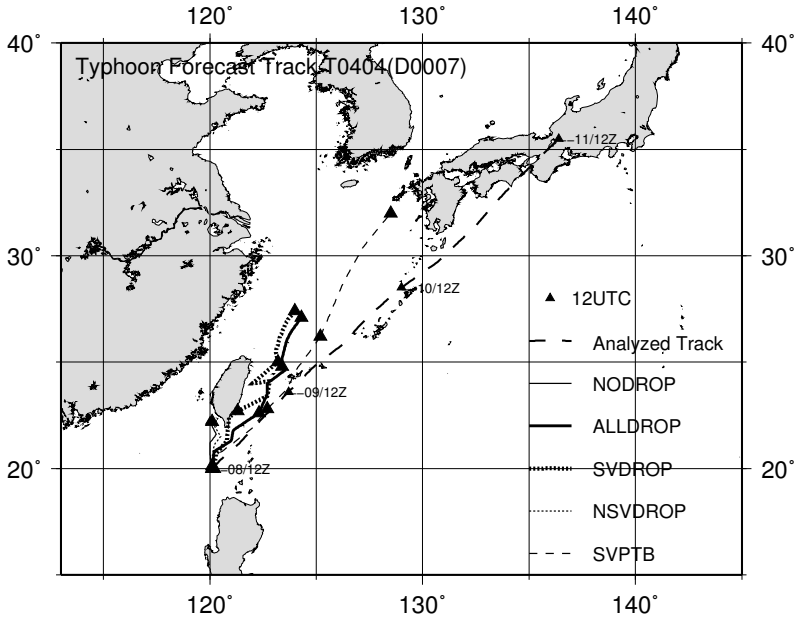

FIG. 4. Results of OSE-1, OSE-2 and SVPTB. The thick (thin) solid line is track prediction from ALLDROP (NODROP), the thick (thin) dot line is for SVDROP (NSVDROP), and the short dashed line is for SVPTB. The long dashed line is the analyzed track of Conson. The triangles on each track are plotted every 24 hour.

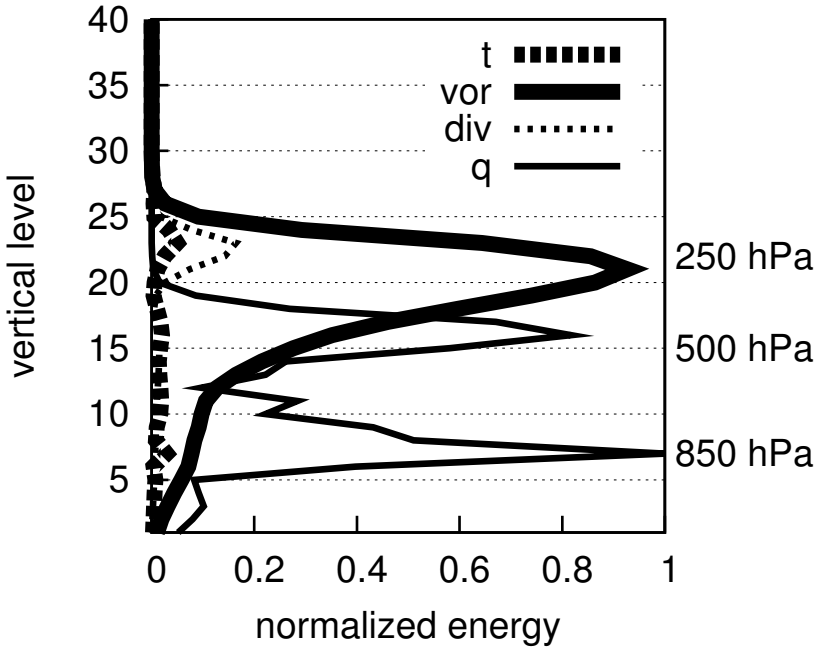

FIG. 5. Analysis increments resulting from assimilating all observations in ALLDROP. They are represented as a form of the vertical distribution of each component of the total energy. Vertical level 7 almost corresponds to 850 hPa, level 15 does 500 hPa and level 22 does 250 hPa. Amplitudes are normalized by the peak value of all variables and all model levels.

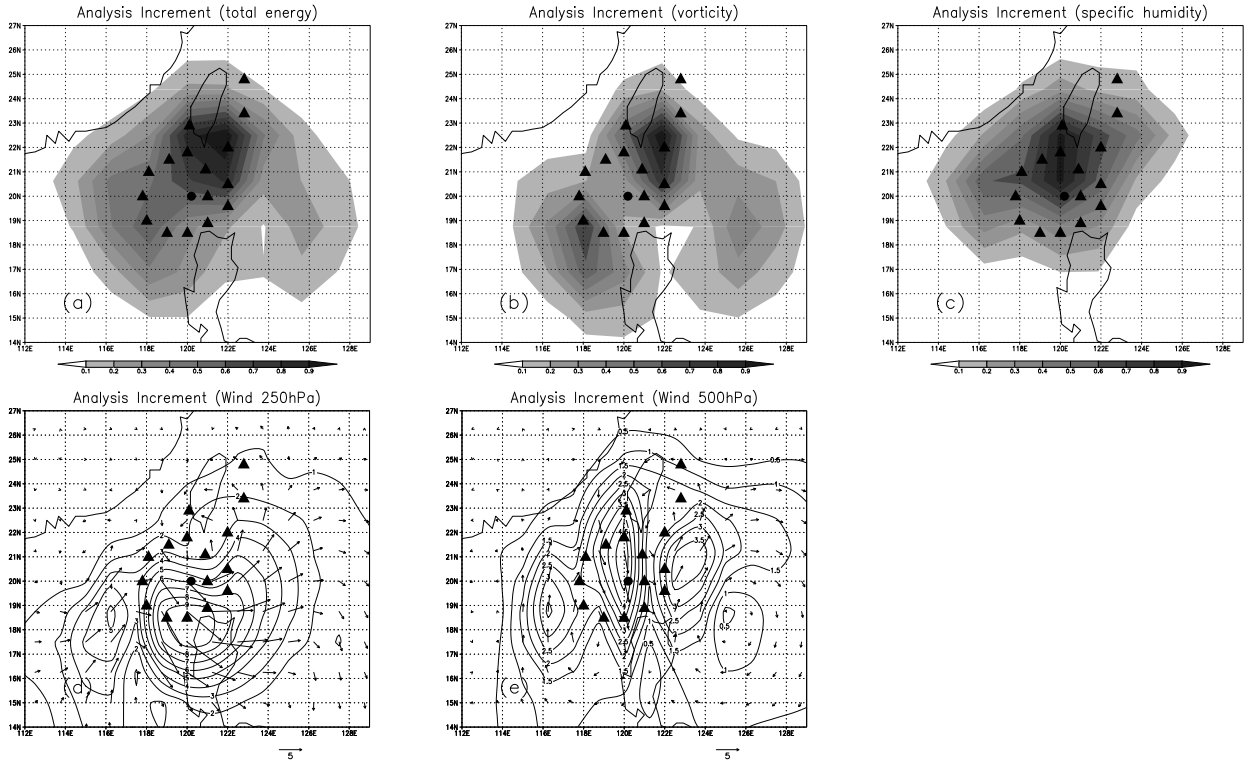

FIG. 6. Horizontal distributions of the analysis increments in ALLDROP. (a) represents the vertically accumulated total energy of the analysis increments. (b) and (c) are its vorticity and specific humidity component. (d) and (e) are wind vectors and isotachs at 250 hPa and 500 hPa, respectively (the vector scale is shown at lower right on each figure, and the unit is m s^{-1}). In (a), (b) and (c), amplitudes are normalized by the maximum value of the whole filed. The black dot and rectangles represent the analyzed central position of Conson and the observation points, respectively.

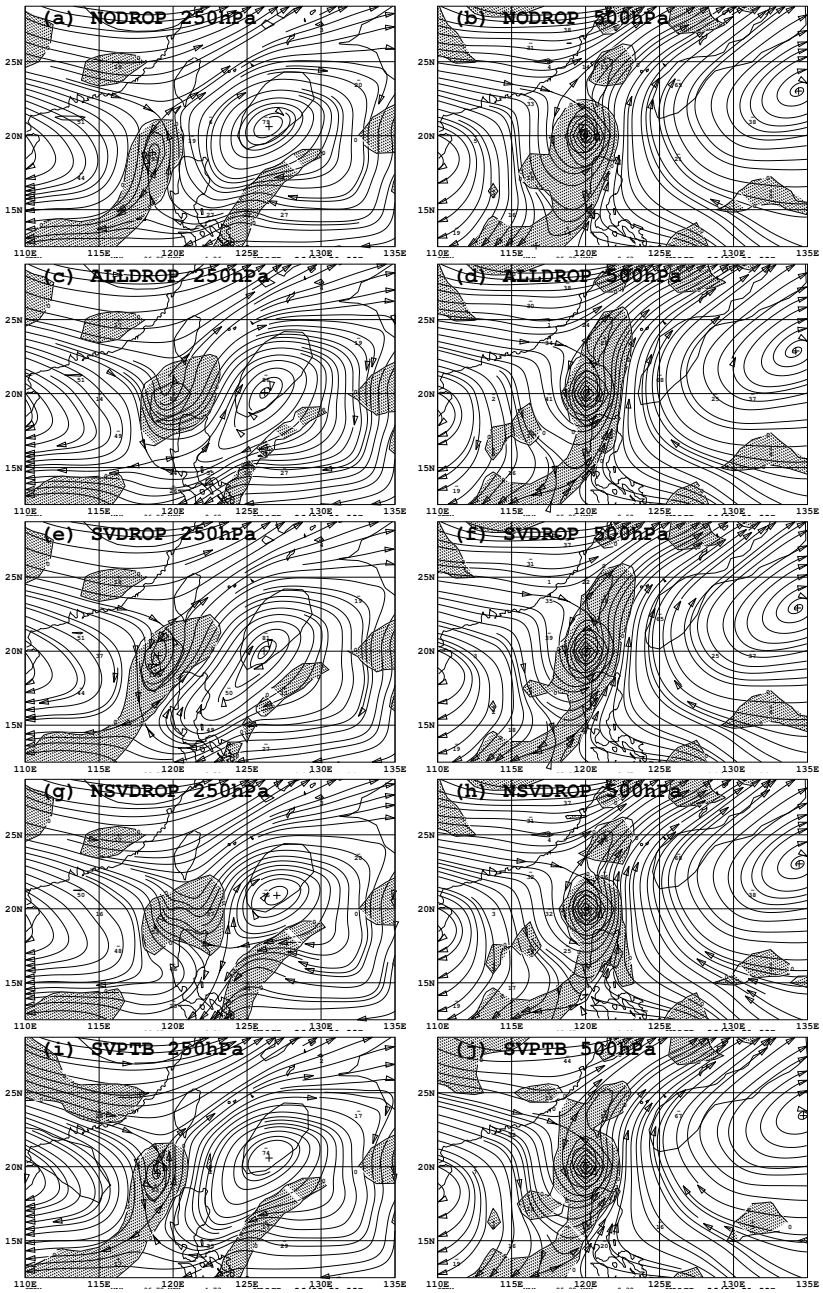

FIG. 7. Initial fields of NODROP, ALLDROP, SVDROP, NSVDROP and SVPTB, regarding vorticity (shaded, unit: 10^{-6} s^{-1}) and streamline (arrow) at 250 hPa (left) and 500 hPa (right).

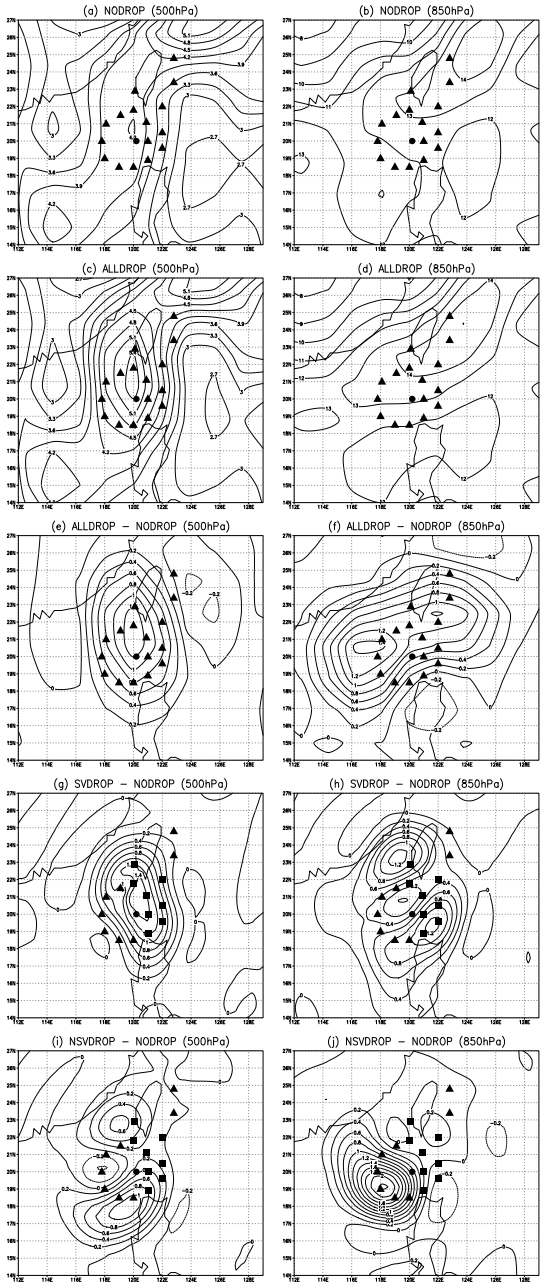

FIG. 8. Initial fields of NODROP and ALLDROP and differences from NODROP, regarding specific humidity (g kg^{-1}) at 500 hPa (left) and 850 hPa (right). In (a) - (f), the triangles represent observations assimilated in ALLDROP. In (g) - (j), the squares and triangles represent observations assimilated in SVDROP and in NSVDROP, respectively. The black dot represents the analyzed central position of Conson (same symbols will be used in Fig. 9, 11 and 12).

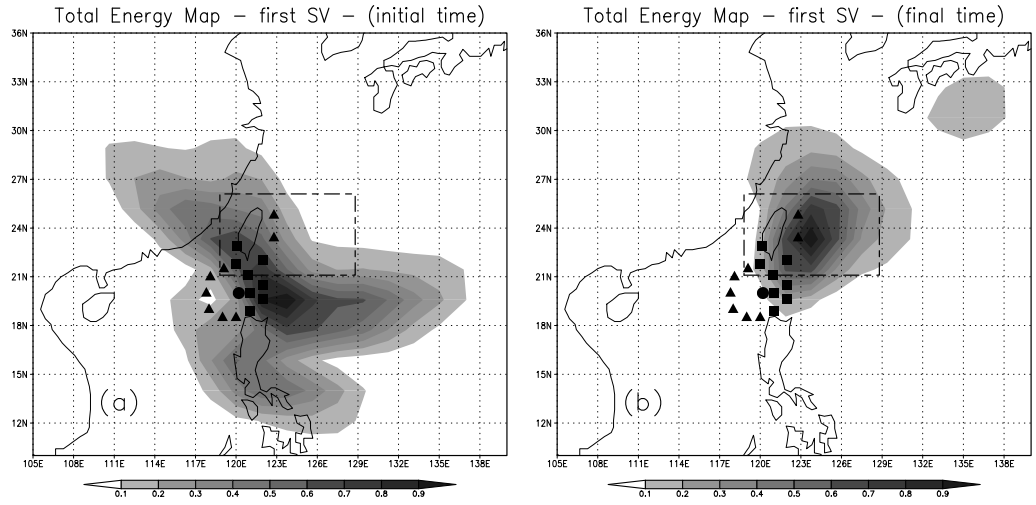

FIG. 9. Vertically accumulated energy of the first moist SV at (a) the initial time and (b) the evaluation time. Amplitudes in both figures are normalized by the maximum value in each field. The dash rectangle shows the targeted area for the SV calculation.

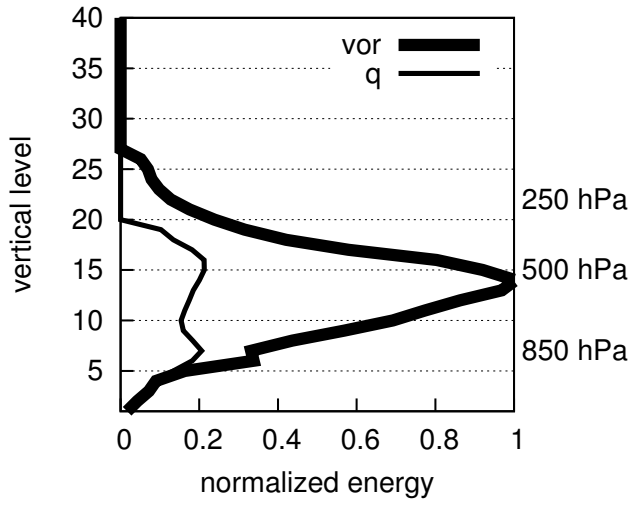

FIG. 10. Vertical energy distribution of the first moist SV at the initial time. The thick line represents the vorticity component of energy and the thin line does the specific humidity component. Vertical level 7 almost corresponds to 850 hPa, level 15 does 500 hPa and level 22 does 250 hPa. Amplitudes are normalized by the peak value of the two variables and all model levels.

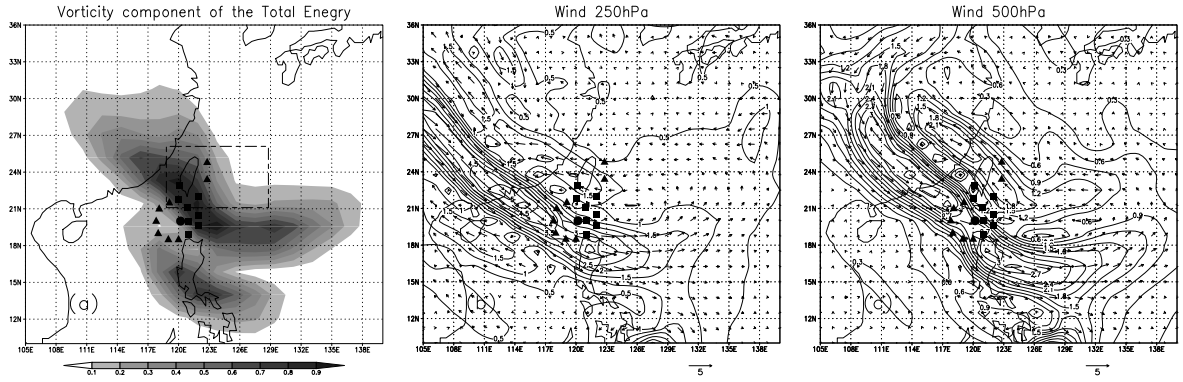

FIG. 11. (a) Vertically accumulated vorticity component of energy of the first moist SV at the initial time. (b) and (c) show the wind vectors and isotachs at 250 hPa and 500 hPa, respectively. In (a), amplitudes are normalized by the maximum value in the whole field, and in (b) and (c), amplitudes are adjusted in the same way as the Typhoon Ensemble Prediction System at JMA (the vector scale is shown at lower right on each figure, and the unit is m s^{-1}). The dashed rectangle in (a) shows the targeted area for the SV calculation.

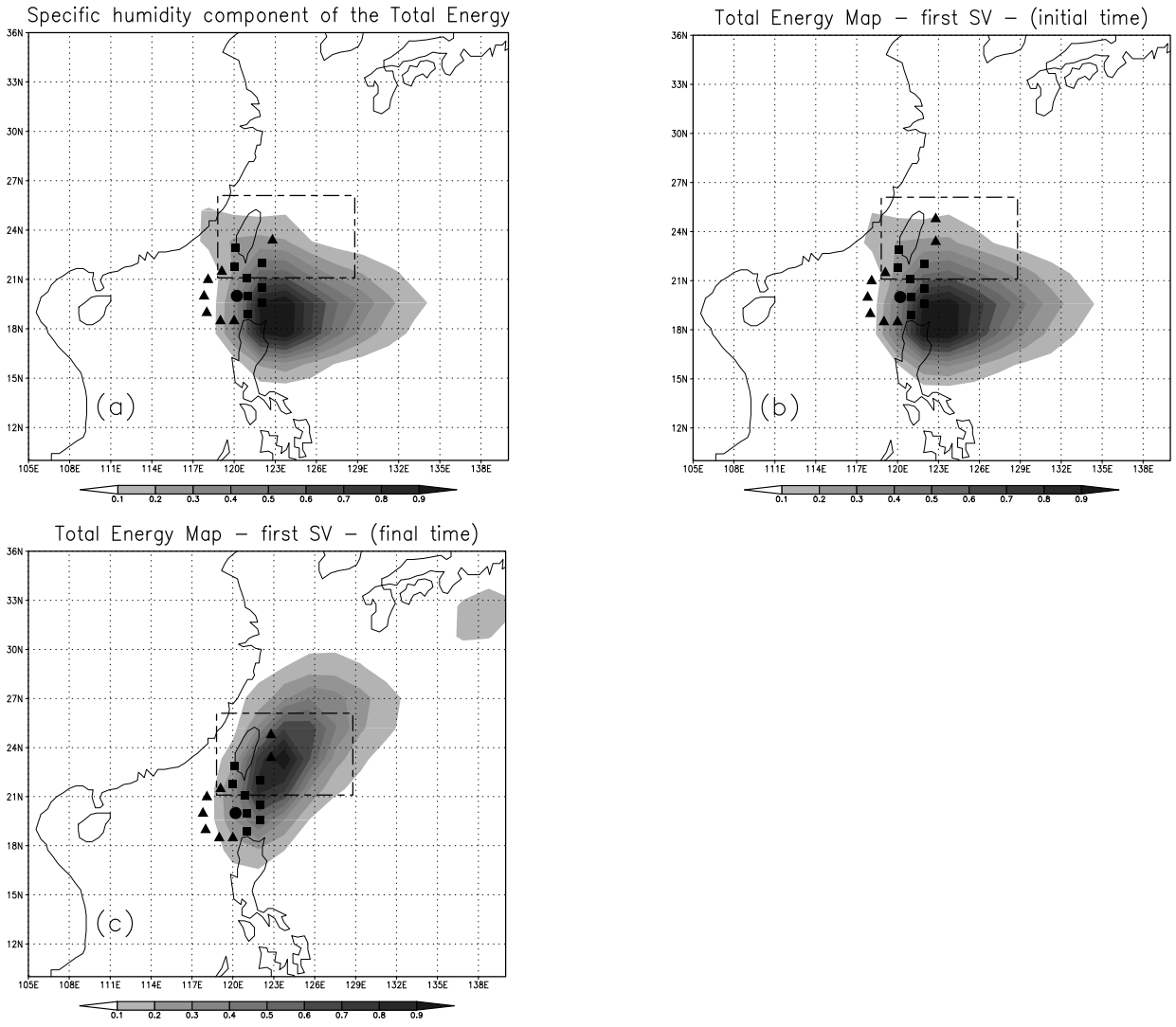

FIG. 12. (a) Vertically accumulated specific humidity component of energy of the first moist SV at the initial time. (b) and (c) show that of an initial and final SV that are calculated under the condition that only the effect of specific humidity component of energy is considered in a formulation of an initial norm. Amplitudes are normalized by the maximum value in each field. The dashed rectangle shows the targeted area for the SV calculations.

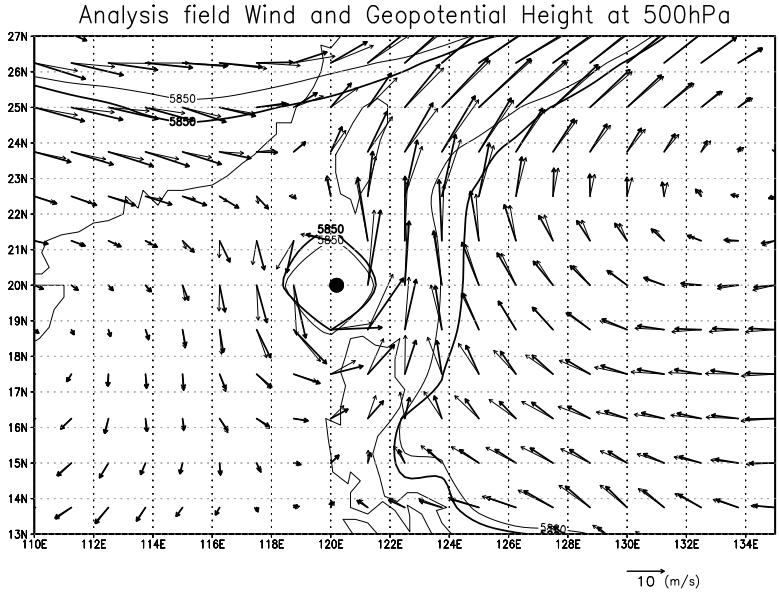

FIG. 13. Comparison of the initial fields between NODROP (thin) and SVPTB (thick) regarding wind (arrow, unit: m s^{-1}) and geopotential height (line, unit: m) at 500 hPa.

List of Tables

TABLE 1. Position errors (km) of 24, 48 and 72 hour forecasts at each experiment.

	24-h	48-h	72-h
NODROP	410	-	-
ALLDROP	181	692	1479
SVDROP	265	692	1479
NSVDROP	400	-	-
SVPTB	135	454	827